Egypt. J. Chem. **Vol 64**, No10, pp 5765 - 5780 (2021)

Egyptian Journal of Chemistry

http://ejchem.journals.ekb.eg/

Effect of Ruthenium promotor ratio on Ni/Y_2O_3 Based Catalysts for CO_2 Methanation Reaction

Radwa A. El-Salamony[*1], Sara A. El-Sharaky[1], Seham A. El-Temtamy[1], Ahmed M. Al-Sabagh[1], Hamada M. Killa[2]

[1]*Egyptian Petroleum Research Institute (EPRI), Cairo, Egypt*

[2] *Faculty of Science, Al-Zagazig University, Cairo, Egypt*

Abstract

CO_2 is one of the main contributors to the greenhouse effect and hence to climate change, there is a growing interest in its use as a feedstock in chemical processes. CO_2 methanation has recently gained renewed interest. A series of nickel supported on yttrium oxide and promoted with different ratios of ruthenium was prepared by the wet impregnation method. The developed Ru-Ni/Y_2O_3 structure was then characterized using N_2 adsorption-desorption isotherm, XRD, XPS, TPR, and HTEM techniques to evaluate the surface, crystal phase, and morphology. The catalytic test was conducted with the use of a fixed-bed tubular reactor under atmospheric pressure. Temperature of catalytic performance was 350 °C with a supply of CO_2/H_2/Ar with a ratio of 1/4/5 and a total flow rate of 200 ml/min. The main products of the reaction were CH_4 and water. Traces of carbon monoxide was present among the product. The methane yield was reached 16.4%, 14%, 17.74%, and 14.24% over Ni/Y_2O_3, 1Ru-Ni/Y_2O_3, 5Ru-Ni/Y_2O_3, and 10Ru-Ni/Y_2O_3 catalysts respectively. The amount of promoter was stated to have affected the catalytic activity but huge numbers usually of promoters diminishing catalytic activity due to active site coverage. However; the increase in Ru loading in the 10Ru-Ni/Y_2O_3 sample decreased the catalytic activity towards methanation due to the Ru-precursor used ($RuCl_3.nH_2O$) in this study. The residual chloride ions form a barrier between the support and the metal, and thus both inhibit CO and hydrogen chemisorption on the catalyst surface.

Keywords: Ru-Ni bi-metal, CO_2 hydrogenation, Methanation, Yttrium oxide, Water.

1. Introduction

Hydrogen is a clean and efficient fuel, which has the least pollutant impact on the air that can be produced through steam reforming [1–4] and renewable energy such as solar energy [5,6], has attracted a great deal of attention to relieve the heavy dependence on fossil fuel in the future. To overcome the hard work to transport and store hydrogen a lot of researchers have investigated the carrier for hydrogen [7, 8].

On the other hand, CO_2 emissions cause the loss of vast quantities of carbon, which is the building block of fossil fuels and petrochemicals. The technology most widely studied to reducing CO_2 emissions is carbon capture and sequestration (CCS) consisting of CO_2 capture, transport, and underground storage. Instead, the CO_2 collected may be used and converted into fuels and chemicals such as dry methane reforming for the manufacture of synthesis gas [9–11] or CO_2 hydrogenation to CH_4 [12–17], methanol, or higher alcohol [18–20].

Methane, the primary component of natural gas, can be transported using the proven networks of pipelines. In addition to being a fuel, methane is also an essential chemical material [21].

The hydrogenation of CO_2 or methanation, also called the Sabatier reaction, was first studied in the early last century by Sabatier and Senderens [22]. The early application of such a process was for ammonia synthesis to extract trace carbon oxides from the feed [23, 24]. Due to its use in the so-called Power-to-Gas technology [25] as well as biogas upgrading [26], CO_2 methanation has recently gained renewed interest.

The conversion of carbon dioxide with hydrogen is a well-known exothermic reaction, which is typically carried out at moderate temperatures (250–350 °C), the ideal H_2: CO_2 ratio is 4: 1, and pressures (5–25 bar g) through heterogeneous catalysis [27, 28]. However, the CO_2 reduction process owns high kinetic barriers, making this process difficult to achieve, and CO_2 is so stable that difficult to be

*Corresponding author e-mail: radwa2005@hotmail.com
Receive Date: 08 December 2020, Revise Date: 06 May 2021, Accept Date: 23 May 2021
DOI: 10.21608/EJCHEM.2021.51324.3072

activated [29–31]. Therefore, CO_2 activation and conversion at low temperatures is a critical challenge. The mechanisms proposed for CO_2 methanation according to the studies from experimental works and theoretical calculations can be divided into two categories. The first one involves that CO_2 will be converted to CO by reverse water gas shift (RWGS) reaction followed with CO methanation [8,14,32]. The other mechanism is the direct hydrogenation of CO_2, which is related to the formation of intermediate such as formate species [33].

In methanation reaction heterogeneous catalyst is based on two commercial materials, nickel as active phase and γ-alumina as support, which is used to disperse the active phase and confer stability to the whole catalyst [12]. However, supported nickel catalysts continue widely studied materials. The nature of support plays a crucial role in the interaction between the nickel and the support, and thus determines catalytic performances toward activity and selectivity for the methanation of CO_2 [34].

Besides γ-alumina, another supports such as Y_2O_3, Sm_2O_3, ZrO_2, ZnO and CeO_2 provide better properties to nickel-based catalysts, which consequently exhibit higher catalytic activity [14,17,35–39].

The shortages of the Ni-based catalyst are poor activity at low temperature and the sintering of Ni nanoparticles (NPs) at high temperature [40]. The problem of Ni-based catalysts is their deactivation at low temperatures due to the interaction of the metal particles with carbon monoxide and the formation of mobile nickel sub carbonyl [41]. Therefore, developing catalyst with high activity at low temperature and good resistance to sintering is the focus for CO_2 methanation. To overcome this problem, the addition of second metals such as Ce [42,43], Zr [44,45], La [46,47], Mo [48], and Mg [15,49] has been attempted to enhance the stability and catalytic activity of the nickel-based catalysts [50].

Finch and Ripley [51] claimed that the noble metal promoters such as Rh, Ru, Pt, and Pd may enhance the activity of the catalysts and maintained greater activity for methane conversion than non-promoted catalysts.

Ruthenium, although more expensive, is more active and stable at operating conditions for CO_2 methanation than nickel [52]. Ru/Al_2O_3 catalysts are highly selective towards methane, and the main products of the reaction were CH_4 and water. Traces of carbon monoxide were present among the product, too, but methanol was completely absent [53]. The selectivity to methane achieved maximum when the Ru loading was increased to 10 wt%, which was attributed to the sintered phase of Ru on the Al_2O_3 support [54].

However, another study found a small amount of methanol was produced on Raney Ru catalysts [55], but the production of methane gas was thousands of times more than the amount of methanol from CO_2 hydrogenation. Also; the addition of noble metals on Ni resulted in a decrease in the reduction temperature of Ni and an increase in the amount of H_2 uptake on Ni on the catalyst [56–58]. Under steady-state conditions, the reaction rate determined for a highly loaded 15 wt% Ru/Al_2O_3 sample was about 10 times higher than that obtained for the Ni-based system [59]. Furthermore, Luo et al. have studied the effect of yttrium addition on the hydrogenation performance and surface properties of a Ru/sepiolite catalyst [60]. The presence of yttrium in Ru/sepiolite aids in increasing the catalytic activity and anti-poisoning capacity of the catalyst. The addition of yttrium increases the active surface area and the dispersion of ruthenium.

Ru can also be combined with Ni to form a bimetallic methanation catalyst, which showed many enhanced performances [61,62] found that the segregation of Ru on the $Ni–Ru/\gamma\text{-}Al_2O_3$ catalyst surface could provide more active Ru species. Therefore, adding a small amount of Ru in Ni catalyst is a promising way to promote methanation reaction for long time stability and high activity [63]. Recently; Y_2O_3, an effective metal oxide, was used in a wide range of areas vary due to its optical, thermal, and chemical stabilities [64–68].

In the present work, we evaluate the influence of using ruthenium metal oxide at a different loading level of 1%, 5%, and 10% wt/wt as promoters on $10\%Ni/Y_2O_3$ catalyst by co-precipitation method. The effect of promoter on the morphology and catalytic activity towards CO_2 methanation reaction is examined under atmospheric pressure and 350 °C using H_2: CO_2 of 4.

2- Experimental

2.1. Materials

Yttrium Oxide (Y_2O_3), 99.9% AR is precached from Loba Chemie (Mumbai, India), M. Wt. 225.81. It calcined at 500 °C for 4 hours.

Nitrate precursors, nickel nitrate hexahydrate $Ni(NO_3)_2.6H_2O$, and ruthenium (III) chloride hydrate $RuCl_3.xH_2O$, 99.9% is precached from Acros Organics-Thermo Fisher Scientific (New Jersey, USA).

2.2. Preparation method

All catalysts were prepared by the wet impregnation method [57]. Three grams of calcined yttrium oxide support was prepared per batch. Nickel nitrate hexahydrate is used as the base in this research and ruthenium (III) chloride hydrate is used as a promoter. Typically; nickel nitrate and ruthenium chloride were dissolved separately in distilled water at room temperature. Yttrium oxide support was weighed and added to the aqueous solution. Then, the mixture was kept on a bath at 80 °C under slow stirring until complete evaporation, for 4 h. The impregnated material was kept at 110 °C in an atmospheric oven overnight. Then, the catalysts were calcined at 500 °C for 4 h. The nominal nickel loading amount was fixed at 10 wt% and the ruthenium promoter at 0, 1, 5, 10 wt%. The prepared catalysts were labeled respectively as 10Ni/Y_2O_3, 1Ru-Ni/Y_2O_3, 5Ru-Ni/Y_2O_3, and 10Ni-10Ru/Y_2O_3.

2.3. Catalysts Characterization

Textural properties of the catalysts were determined by N2-physisorption (NOVA 3200 apparatus, Quantachrome Corporation, Boynton Beach, Florida, USA) at -196˚ C. Before the measurements, the samples were degassed at 250 °C for 4 h. Brunauer-Emmett-Teller (BET) method was used to calculate the BET surface area for a relative pressure ($P/P_\circ$) range between 0.05-0.30. Barrett-Joyner-Halenda (BJH) method was applied to desorption.

The crystalline structure and the different phases of nanoparticles were investigated via X-ray diffraction analysis (XRD) using Shimadzu XD-1 diffractometer, Germany. The wide-angles data were obtained using a Cu Kα radiation (λ=1.5406 Å). The diffraction acquisitions were done in a range from 20 to 80°. The crystalline phase was identified by using International Centre for Diffraction Data.

The morphology and microstructure of the materials were observed on a transmission electron microscopy (JEOL-2100F), 120 Kw, Japan, attached with (EDX) Oxford X-Max. This technique offered high-resolution electron imaging up to 0.143 nm and high magnification up to 1.5 million times

The reducibility of the calcined catalysts was studied by H2-Temperature programmed reduction (Quantachrome equipment, USA). H_2-TPR was conducted using an H_2: Ar (5/95 vol%) mixture as the reducing gas at a flow of 30 mL min^{-1} in the temperature range of 35–1000 °C at a heating ramp of 10 °C min^{-1}. The amount of H_2 uptake was measured with a thermal conductivity detector.

Chemical valence states of the samples were determined by an X-ray photoelectron spectroscopy (XPS); K-ALPHA Surface Analysis, Thermo Scientific USA. The spectrometer is equipped with monochromatized Al Ka. The sample was mounted on the standard sample stubs using double-sided adhesive tapes. The core level signals were obtained at a photoelectron take-off angle (R, measured for the sample surface) of 908. The X-ray source was run at a reduced power of 150 W (15 kV and 10 mA). The pressure in the analysis chamber was maintained at 10^{-8} Torr or lower during each measurement.

2.4. Catalytic activity

Carbon dioxide hydrogenation was carried out in a fixed volume flow tubular homemade reactor operating at atmospheric pressure. The quartz silica reactor was heated in an electric furnace equipped with a programmable temperature controller. 2 gm of fresh catalyst was diluted with silicon carbide to obtain 5cm bed height and packed in the middle of the reactor. The temperature was monitored by a K-type thermocouple placed in the center of the catalyst bed. Before the catalytic test, all the samples were activated in situ with a 30 ml/min flow of pure hydrogen at atmospheric pressure for 1 h at 600 °C. After the reduction, the catalysts were cooled down and a flow of premixed gas at a molar ratio of $CO_2/H_2/Ar$ = 1/4/5 with a GHSV of 6000 $ccg^{-1}h^{-1}$ was gradually introduced through the catalysts. Then, the temperature was increased to 350 °C and the reaction time was 3h. Gaseous reaction products were analyzed online by a quantitative gas analysis system (HIDEN ANALYTICAL QGA, England). The selectivity of H_2, CO_2, CH_4 and, CO was detected by gas analyzer using a matrix equation to correct the overlapped detection values from the m/z of 28 (CO), 44 (CO_2), 2 (H_2), and 16 (CH_4).

The carbon dioxide (CO_2) conversion was calculated by:

$$\frac{[CO2]_{in} - [CO2]_{out}}{[CO2]_{in}}$$

The methane (CH_4) yield was calculated by:

$$Y_{CH4} = \frac{X_{CO2}\, x\, S_{CH4}}{100\%}$$

The carbon monoxide (CO) yield was calculated by:

$$Y_{CO} = \frac{X_{CO2}\, x\, S_{CO}}{100\%}$$

Whereas S_{CH4}, S_{CO}, X_{CO2} are the selectivity of methane, carbon monoxide, and conversion of carbon dioxide respectively [69].

2. Results and discussion:

2.1. X-ray diffraction analysis

XRD patterns of yttrium oxide-based catalysts are presented in Fig.1. Distinct XRD peaks indexed to the cubic phase of Y_2O_3 were observed for all the samples. The patterns show the intense peaks at 2θ values of 29.14°, 33.77°, 48.51°, and 57.57° according to JCPDS card no.: 04-005-4378 characteristic to cubic YO structure [70]. The characteristic diffraction peaks of NiO at 2θ = 37.2, 43.3, and 62.8° cannot be seen in the Ni/Y_2O_3 catalyst. It demonstrated that Ni species were well dispersed on the Y_2O_3 surface due to the existing overlaps peaks of NiO and Y_2O_3 of XRD pattern are difficult to differentiate [71].

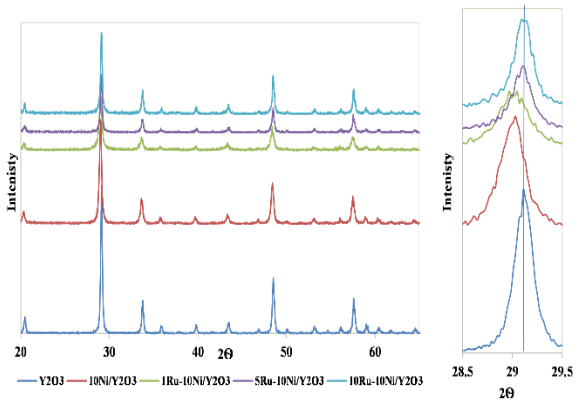

Fig. 1. XRD patterns of yttrium oxide-based catalysts

However; the diffraction peaks at 28.0°, 35.1°, and 54.4° of tetragonal RuO_2, and the three peaks at 38°, 44° and 69° of the metallic Ru [72] weren't detected in $1Ru-Ni/Y_2O_3$, $5Ru-Ni/Y_2O_3$ catalysts. This is related to the uniformly and finely dispersed of the metals over the support surface using the wet impregnation method [73]. This result was also noticed by Basahel et al., [74], El Naggar et al. [75], and El-Salamony et al. [76]. They reported that there are no reflections due to crystalline CuO phase were observed in XRD pattern of 10-CuZr sample [74] and a complete absence for any sharp MoO_3 characteristic peaks in 10Mo-SBA-15 and 15Mo-SBA-15 catalysts [75,76]; respectively suggesting that CuO might be well dispersed on the surface of ZrO_2 support [74] and MoO_3 segregated as an amorphous phase within the silica matrix and there is the non-existence of the crystalline domains of copper oxide rather than molybdenum oxide, unless of being present with crystal sizes that are too small to be detected at the high angle X-ray diffraction [1,74–76]. The two catalysts $5Ru-Ni/Y_2O_3$ and $10Ru-Ni/Y_2O_3$ had exhibited characteristic peaks of NiO with elevated intensities in their XRD patterns, as illustrated in Table 1.

Table 1: XRD data for $5Ru-Ni/Y_2O_3$ and $10Ru-Ni/Y_2O_3$Catalysts

Catalysts	Pos. [°2θ]	Height [cts]	FWHM Left [°2θ]	d-spacing [Å]
$5Ru-Ni/Y_2O_3$	29.2961	15.38	0.1968	3.04862
	37.4979	7.14	0.3149	2.39852
	43.357	20.25	0.551	2.08701
	48.7073	8.52	0.3936	1.86954
	57.822	6.03	0.4723	1.59466
	62.8203	9.04	0.551	1.47927
$10Ru-Ni/Y_2O_3$	29.1972	3.05872	62.46	0.2755
	33.8344	2.64936	16.4	0.2362
	35.2595	2.54548	3.96	0.2558
	37.4119	2.40383	6.43	0.3346
	40.021	2.25294	2.71	0.9446
	43.4734	2.08169	15.75	0.3936
	48.6959	1.86995	30.42	0.1968
	53.3012	1.71874	3.75	0.4723
	57.8067	1.59504	20.78	0.2558
	59.1525	1.56193	4.43	0.4723
	60.5555	1.52905	3.72	0.4723
	63.0007	1.47547	5.9	0.3149

Besides only one peak characteristic to RuO_2 in the case of the $10Ru-Ni/Y_2O_3$ sample. The insets of Fig. 1, give an expended view of the main peak. It is indicating a shift of the reflection peaks in the case of Ni/Y_2O_3 and $1Ru-Ni/Y_2O_3$ samples and peak broadening in the case of bi-metal samples after Ru ion implantation with different doses. The lattice distortion resulting from crystal deficiencies may lead to a shift in the position reflections [77]. In the case of bi-metal samples, there is only peak broadening which also reflected a change of microstructure in the implanted samples with an increasing implantation dose of Ru ion.

2.2. Catalytic surface area properties

The nitrogen adsorption/desorption isotherm curve as well as the pore size distribution (the inset picture) of the yttrium oxide-based catalysts are shown in Fig. 2. The isotherm of catalysts classified to type IV

isotherm indicating to the formation of mesopores material on the support during the preparation method [78]. They exhibited an H3-type hysteresis loop, however, the H3 loop does not have a plateau at high P/P_o. The yttrium oxide support exhibits the same shape as a type II isotherm (Supplementary data S1). This pseudo-type II character is associated with low surface area, porosity, and unrestricted monolayer-multilayer adsorption [79] and is due to the low degree of pore curvature. This encourages the impregnation of the metal oxides on the surface and wall interacting of the support to form a multilayer with definite porosity. This discusses the increase of the surface area of the prepared sample in comparison to Y_2O_3 support. The corresponding BET-specific surface area is represented in Table 2. The surface area decreased by increasing Ru metal loading and the same applied to pore volume and pore diameter this due to the large ionic radius of Ru^{+3} (0.85 nm) comparison to that of Ni^{+2} (0.7 nm) which decrease the porosity of amorphous oxide formed during the preparation procedure. Using the BJH method the pore diameter distribution is obtained (Fig. 2). It demonstrated that the catalysts possessed uni-modal wide-ranging pore distribution from micro- to meso-pore with pore width from 0.2 to 6 nm. which is typical for mesoporous material [80].

Table 2: Texture properties of the prepared catalysts

Catalysts	Surface Area S_{BET} (m^2/g)	Total Pore Volume (cc/g)	Pore Diameter (nm)
Ni/Y_2O_3	15.5	0.0701	12.34
$1Ru\text{-}Ni/Y_2O_3$	14.93	0.0771	2.82
$5Ru\text{-}Ni/Y_2O_3$	14.44	0.0601	2.39
$10Ru\text{-}Ni/Y_2O_3$	10.62	0.0514	0.986

Fig. 2. N2 adsorption/desorption isotherm and pore size distribution (inside Figs.) of the yttrium oxide-based nano-catalysts.

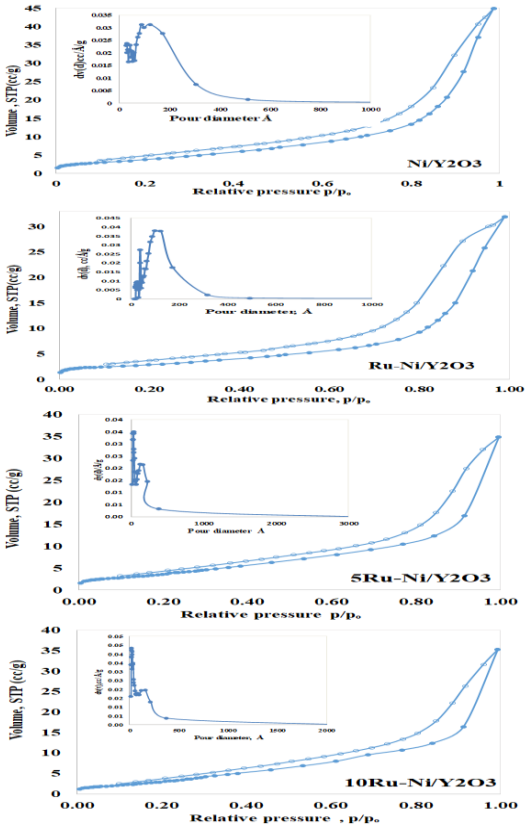

2.3. Temperature Programmed Reduction (TPR):

The reduction behaviors of yttria-based catalysts were measured by TPR at the temperature range 50-1000 °C, and the results are shown in Fig. 3. Generally, the reduction temperatures of NiO reflected the interactions between NiO and supports [81, 82]. As for Y_2O_3 support, a weak reduction peak centered around 600 °C has been reported that it could be partially reduced due to the lattice oxygen on its surface [83–85]. For Ni/Y_2O_3 sample the reduction peaks at T_{max} of 312, 373, and 418 °C assigned to the reduction of NiO and support interacting NiO, respectively, to metallic Ni [86] corresponding presumably to NiO nanocrystals of various sizes [87]. The hydrogen consumption values and T_{max} during the TPR of the prepared catalysts are reported in Table 3.

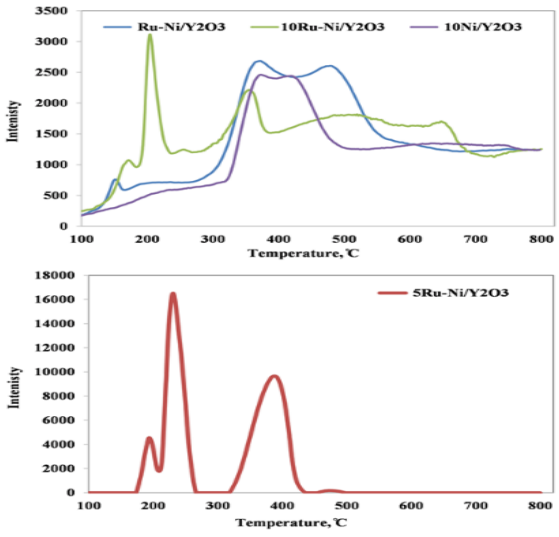

Fig. 3. H2-TPR of the prepared catalysts

The H_2-TPR profile of the bi-metal Ru-Ni based-catalysts exhibited reduction peaks at T_{max} 171, 230, 204, 255, and 273 °C characteristics to the reduction peaks of RuO_2 to Ru metal, which is in agreement with the results reported in many literatures [88–94] However; the 1Ru-Ni/Y_2O_3 sample is also detected, which match to ruthenium oxychloride [95]. In addition, the reduction profiles of NiO on the prepared catalysts have been detected and they generally point to the presence of two NiO species, one interacting strongly with the support and the other weakly. Strong chemical interaction between NiO and the support results in a shift of the reduction peak to higher temperatures *β-type* NiO (350-600 ºC), whereas weak interaction results in reduction at low temperatures assigned to *α-type* NiO species (200-350 ºC) [57,96–98]. The hydrogen consumed of the prepared catalysts was 2.558 mmolg^{-1}, 2.15 mmolg^{-1}, 3.027 mmolg^{-1}, and 3.138 mmolg^{-1} for Ni/Y_2O_3, 1Ru-Ni/Y_2O_3 5Ru-Ni/Y_2O_3, and 10Ru-Ni/ Y_2O_3 catalysts, respectively. H_2-TPR results revealed that the Ru favored the reduction of NiO, probably because they weaken the interaction between Ni and the yttria support, as well this behavior is reported in several studies [57,96].

Table 3: Hydrogen consumption values and T_{max} during the TPR for the prepared catalysts

Catalysts	T_{max} °C	H_2 consumed, mmol/g
Ni/Y_2O_3	312.7	0.274
	373.3	0.468
	418.9	0.672
	632.8	1.144
1Ru-Ni/Y_2O_3	151.8	0.075
	273.9	0.214
	371.3	0.86
	480.1	1.001
5Ru-Ni/Y_2O_3	194.1	0.255
	230.9	0.889
	388.2	1.33
	472.8	0.291
	546.8	0.262
10Ru-Ni/Y_2O_3	171.6	0.13
	204.3	0.27
	255.3	0.147
	354.6	0.638
	519.4	1.221
	647.7	0.732

2.4. Structure of Ru-Ni/Y_2O_3 sample

2.4.1. X-ray Photoelectron Spectroscopy (XPS)

To investigate the chemical state of nickel and ruthenium on the surface of the Y_2O_3 sample XPS measurements were shown in Fig.4. The XPS spectrum of the prepared 1Ru-Ni/Y_2O_3 catalyst shows four major peaks at a binding energy of 159.2 eV, 856.97 eV, 284.89 eV, 532.13 eV assigned to Y3d, Ni2p, Ru3d, and O1s; respectively. The atomic ratios of elements are 26.34%, 7.348%, 1.08% and 58.36%, respectively. The inevitable contaminated peaks are present at 285.91 eV and 199.61 eV due to the hydrocarbon-rich atmosphere, C1s [99] and ruthenium chloride bond, Cl2p [100–103]. The binding energy of Y3d located at 157.7 eV is attributed to $Y3d_{2/3}$ in Y_2O_3 [104]. The peak at159.85 eV characteristic of yttrium trioxalate $Y_2(C_2O_4)_3$ [105]. The Ru3d spectra exhibited three main peaks at 285.99 eV, 289.81 eV, and 283.26 eV. The first peak is representative of $Ru3d_{3/2}$ in Ru-C bond in tetrathiafulvaleneruthenium trichloride dihydrate $(C_6H_4S_4)RuCl_3.2H_2O$ [103], the sound one is assigned to products of hydrocarbon oxidation. Since the 3d band of Ru superimposes the carbon C1s band, the experimental spectral envelope of this region was decomposed by fitting with C1s and Ru3d "synthetic" bands produced with the use of experimentally determined parameters [106]. The last peak is attributed to $Ru3d_{5/2}$ in ruthenium trioxide RuO_3 [101,107].

Table 4: Binding energies and fit parameters for Ni 2p spectra.

Binding Energy (eV)	Name	Line Designation	Formula	Ref.
855.6	Nickel oxide	2p3/2	NiO	[112]
858.2	Ni, sat element	2p3/2	Ni	[113]
874.1	Ni element	2p1/2 sat	Ni	[114]
880.2	Nickelhydroxide	2P1/2 sat	$Ni(OH)_2$	[115]
862.0	Nickel hydroxide	2p3/2 sat	$Ni(OH)_2$	[115]
864.1	Nickel oxide	2p3/2	NiO	[116]

The main peak of Ni at a binding energy of 856.9 eV is assigned to NiO(OH) [108,109]. The detailed

Ni 2p spectra of 1Ru-Ni/Y_2O_3 catalyst were fitted with two major peaks Ni $2p_{1/2}$ and Ni $2p_{3/2}$. The six peaks were fitted in the Ni 2p spectra with binding energies are illustrated in Table 4.

The O1s spectra exhibited three main peaks at 530.43 eV, 531.79 eV, and 532.91 eV. The lower peak at 530.43 eV is characteristic of yttrium oxide Y_2O_3 nanoparticles [110,121]. The peak at 531.79 eV is typical to nickel(II) dihydroxide $Ni(OH)_2$ [107] and the peak at 532.91eV is represented to hydroxyl due to water absorption [112].

2.4.2. TEM-image

Fig. 5. Showed the TEM image at magnification power X30 000 (A), EDX (B), and mapping of 1Ru-Ni/Y_2O_3 sample. Nickel nanoparticles are distributed as a dark round particle on the yttria support the average particle size was 15.06 nm. However; nickel nanoparticles exhibited a strong interaction with yttria support as represented in elemental mapping analysis. While; ruthenium nanoparticles were homogeneous dispersion among the support surface as shown in EMA.

2.5. Catalytic Activity

CO_2 methanation reaction over yttrium-based catalysts was carried out at atmospheric pressure and 350 °C, representative of industrial methanation conditions. The feed gas contains H_2 and CO_2 with a stoichiometric H_2/CO_2 molar ratio of 4. Fig. 6 represents the selectivity % of Ni/Y_2O_3, 1Ru-Ni/Y_2O_3, 5Ru-Ni/Y_2O_3, and 10Ru-Ni/Y_2O_3 catalysts to CH_4, CO, CO_2, H_2, and H_2O components. The selectivity towards CO was decreased as the amount of ruthenium loading increased; as represented in Table 5. Garbarino et al. [113] reported that the catalysts with very small Ni particles are very selective to methane without CO formation. Fig. 6 displays that there is a relation between water formation and the catalytic activity towards methane production. However; the presence of water vapor in the flux of feed caused a negative effect on the CO_2 methanation process. In the case of 1Ru-Ni/Y_2O_3 catalyst, the selectivity of methane decreased to 34.8% due to the formation of a high amount of water (8.2%). This behavior was reported in many studies [23, 114, 115] Whereas; the water vapor decreased the concentration of carbonyl species over the Ni/MSN surface, as shown by IR spectroscopy adsorbed by CO + H_2O [114].

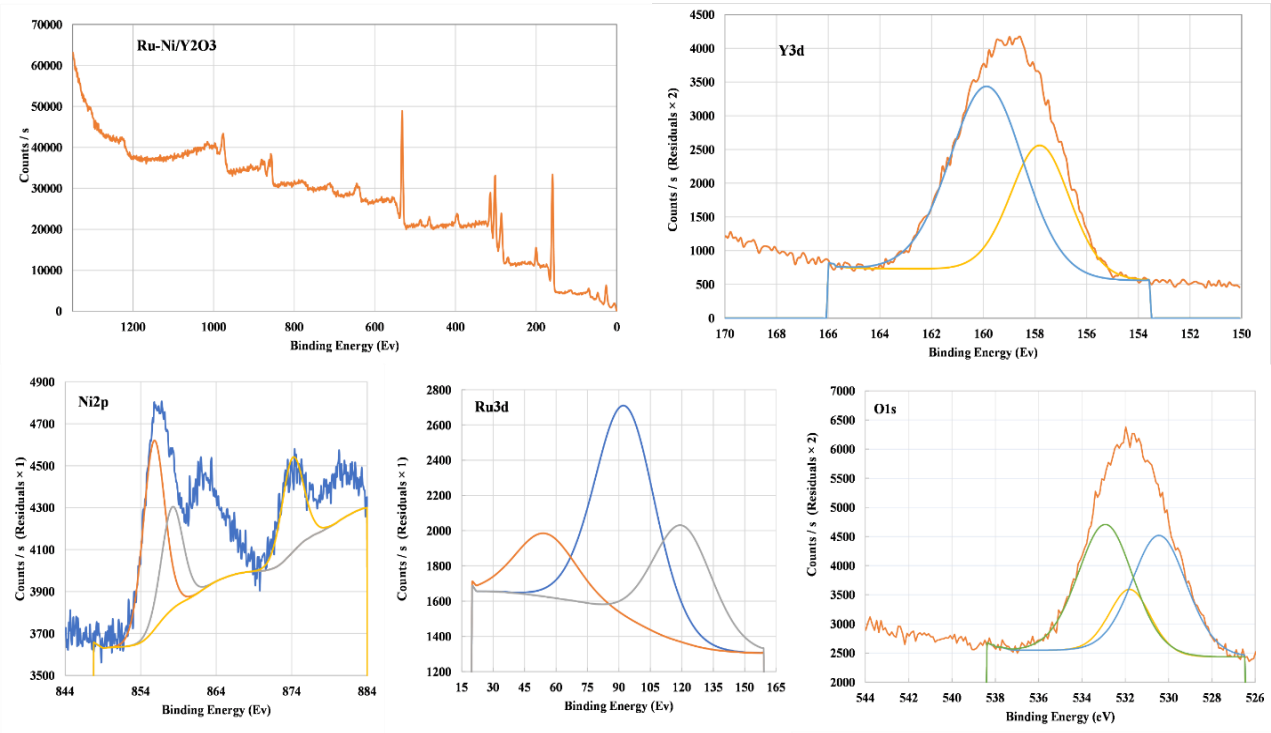

Fig.4: XPS spectra of 1Ru-Ni/Y_2O_3 catalyst

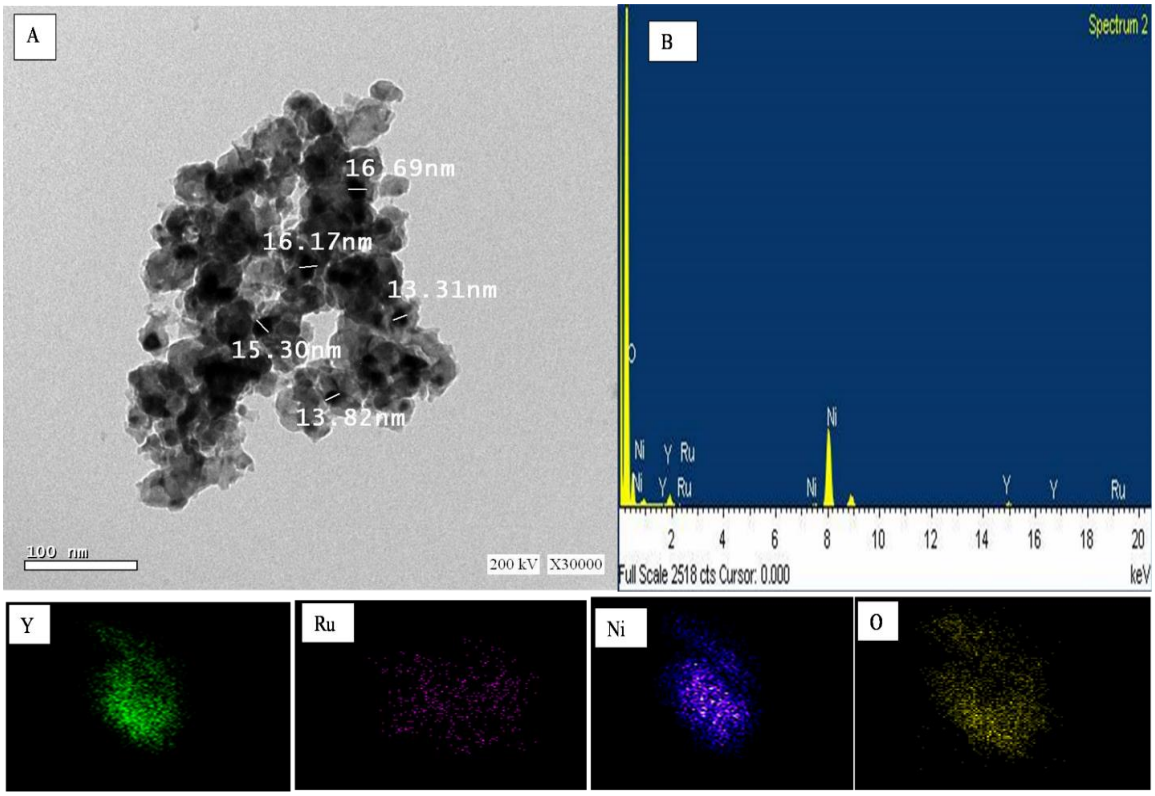

Fig. 5. TEM image of 1Ru-Ni/Y_2O_3 catalyst (A), EDX (B) and elemental mapping analysis (EMA)

Catalytic hydrogenation of CO_2 to methane (Eq. 1) [22,116] is a combination of the reverse water gas shift reaction (Eq. (2)) and CO methanation (Eq. (3)).

$$CO_2 + 4H_2 \leftrightarrow CH_4 + 2H_2O; \quad \Delta H_{298K} = -165\ kJmol^{-1} \quad (1)$$

$$CO_2 + H_2 \leftrightarrow CO_{ad} + H_2O; \quad \Delta H_{298K} = 41\ kJmol^{-1} \quad (2)$$

$$CO_{ad} + 3H_2 \leftrightarrow CH_4 + H_2O; \quad \Delta H_{298K} = -206\ kJmol^{-1} \quad (3)$$

It means that after CO_2 adsorption and dissociation on the surface of the catalyst, CO_2 methanation goes along the same path as CO methanation [117–119]. CO_2 directly dissociated to carbonyl (CO_{ad}) and O_{ad} as intermediates during the methanation process. CO_{ad} subsequently hydrogenated or further dissociated to Cad and O_{ad} in the next step was confirmed over Ru/Al_2O_3 and Ru/TiO_2 catalysts [118,120]. The negative effect was probably due to CO_2 formation through the reaction of the water gas shift (WGS) between the intermediate CO and the excess water. In addition, water vapor significantly accelerates the sintering rate of Ni and increases the collapse of the support, as Bartholomew et al. [97] reported. Batista et al.[121] stated the same trend regarding CO_2 methanation in the Co/γ-Al_2O_3 method, in which reaction occurred not significantly in the presence of water. So, it is proposed that water be present in the feed flux has a detrimental effect on the CO_2 methanation system Ni/MSN system. In addition; Borgschulte et al.[119] reported that water removal from the reaction centers is crucial to improving CH_4's reaction yield and reducing CO release as a side product in its research on CO_2 methanation over nickel catalysts assisted on zirconia. The methane yield achieved a maximum of 17.62 % on the 5Ru-Ni/Y_2O_3 catalyst as the result of zero water formation during the methanation reaction. The increase in CH_4 selectivity could be linked to the methanation reaction preference versus the competitive WGS reaction [122]. Increasing Ru content to 10% further led to increased WGS reaction and formation of water [24].

H_2-TPR profile results confirmed that the addition of 5%Ru increases the reducibility of catalyst which improved the CO_2 conversion and CH_4 yield compared to another catalyst. Also; Tada et al. [42,57] confirmed the enhancement of CO_2 methanation by H_2temperature-programmed reduction that resulting in a partial surface reduction

of CeO_2 on Ru/CeO_2/Al_2O_3 was promoted compared to Ru/CeO_2.

The CO_2 conversions of all the bi-metal catalysts except the 10Ru-Ni/Y_2O_3 sample were higher than those observed for the nickel catalyst. The interaction of two metals could change the electronics and the geometric catalyst structures resulting in more active and stable catalysts via the synergetic effect between Ni and the second metal [96]. The XRD results showed that the loading of the ruthenium diminished the intensities of the diffraction peaks, indicating the formation of small nickel particles with high dispersion on the catalyst surface [123,124]. Besides that higher surface areas of 1Ru-Ni/Y_2O_3 and 5Ru-Ni/Y_2O_3 in comparison to 10Ru-Ni/Y_2O_3 sample could provide more space for Ni dispersion and larger numbers of active sites for methanation reaction. The amount of promoter was stated to have affected the catalytic activity but huge numbers usually of promoters diminishing catalytic activity due to active site coverage [125]. The addition of CeO_2 content up to 2 wt% in Ni/Al_2O_3 catalyst increased the CO_2 conversion markedly as CeO_2 content was increased to 4 wt%, CO_2. The selectivity to CH_4 and CO in the exit gas was almost kept unchanged with increasing CeO_2 content [126]. However; the increase in Ru loading in the 10Ru-Ni/Y_2O_3 sample decreased the catalytic activity towards methanation due to the Ru-precursor used ($RuCl_3.nH_2O$) in this study. That's in good agreement with Nurunnabi et al. [127] and Abu Bakar et al. [58], who found this low chloride ion content in the Ru/Al_2O_3 catalyst might result in a decrease in active Ru catalyst sites surface region. The residual chloride ions form a barrier between the support and the metal, and thus both inhibit CO and hydrogen chemisorption on the catalyst surface.

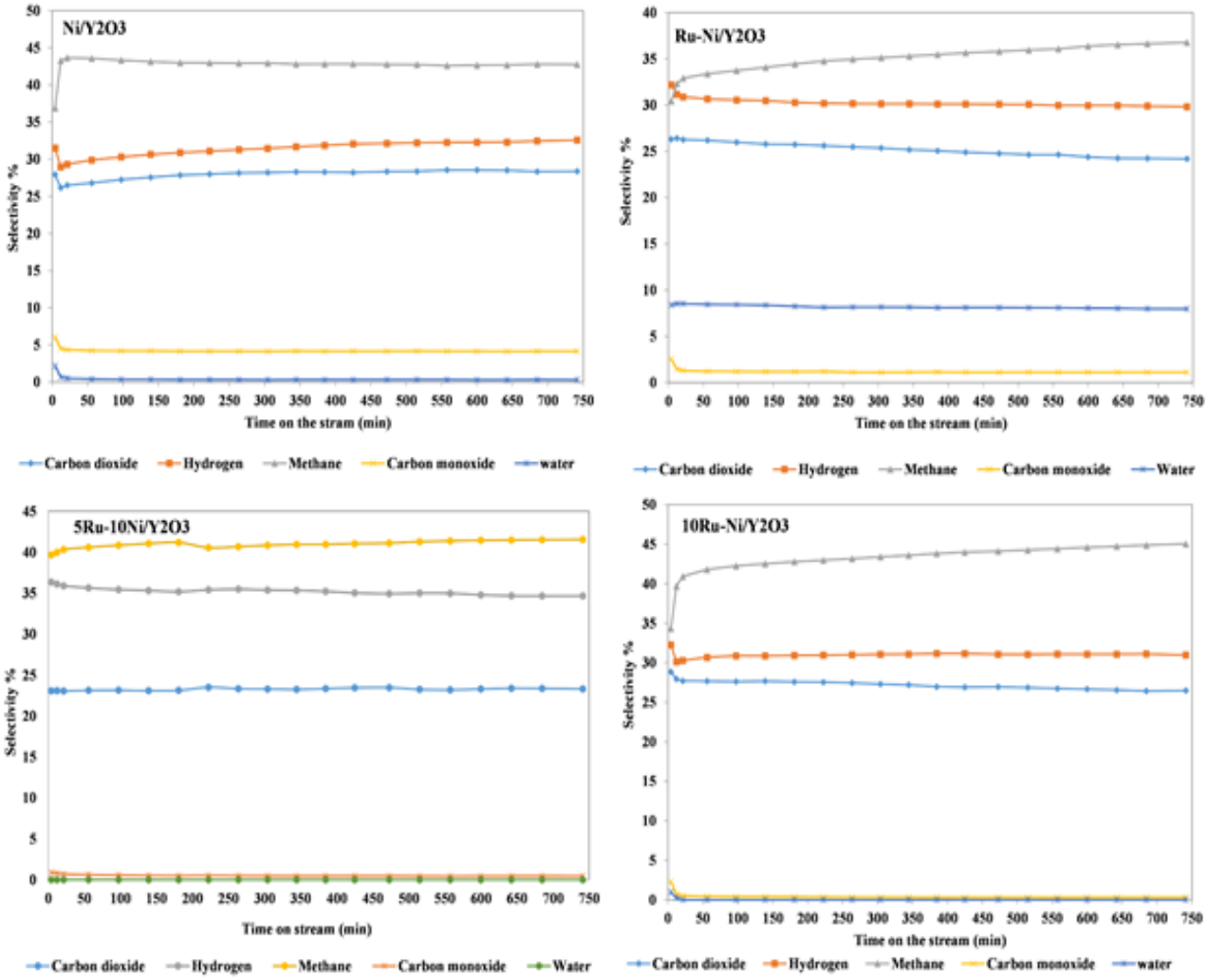

Fig .6. Catalytic performance of Y_2O_3 based-catalysts (molar ratio of H_2: CO_2 = 4, GHSV = 6000 $ccg^{-1}h^{-1}$, T = 350 °C)

Table 5: CO_2 methanation over Ni/Y_2O_3 catalysts at 350 °C and H_2/CO_2 = 4/1.

Catalysts	CH_4 Selectivity %	CH_4 Yield %	CO Selectivity %	CO Yield %	CO_2 conversion
Ni/Y_2O_3	42.7	16.41	4.28	1.7	38.42
1Ru-Ni/Y_2O_3	34.8	14.02	1.23	0.5	40.28
5Ru-Ni/Y_2O_3	40.9	17.74	0.54	0.23	43.38
10Ru-Ni/Y_2O_3	42.8	14.24	0.48	0.16	33.28

3. Conclusion

Nickel supported on yttrium oxide and promoted with three different ratios of ruthenium metal was prepared using the wet-impregnation method and characterized using S_{BET}, XRD, XPS, TPR, and HRTEM/EDX. CO_2 methanation reaction over yttrium-based catalysts was carried out at atmospheric pressure and 350 °C and the feed gas contains H_2 and CO_2 with a stoichiometric H_2/CO_2 molar ratio of 4. The XRD patterns confirmed the uniformly and finely dispersed of the metals over the support surface using the wet impregnation method. H_2-TPR results revealed that the Ru favored the reduction of NiO, probably because they weaken the interaction between Ni and the yttria support. The XPS spectrum of the prepared 1Ru-Ni/Y_2O_3 catalyst shows four major peaks assigned to Y3d, Ni2p, Ru3d, and O1s besides; the inevitable contaminated peaks for C1s and ruthenium chloride bond, Cl2p. The main products of the reaction were CH_4 and water plus traces of carbon monoxide were present among the product. The selectivity towards CO was decreased as the amount of ruthenium loading increased and this was related to the small particle size of a nickel. However; the presence of water vapor in the flux of feed diminished the CO_2 methanation process. The negative effect was probably due to CO_2 formation through the reaction of the water gas shift (WGS) between the intermediate CO and the excess water. In addition, water vapor significantly accelerates the sintering rate of Ni and increases the collapse of the support. The methane yield and CO_2 conversion achieved a maximum of 63.4% and 40.4% respectively; on 5Ru-Ni/Y_2O_3 catalyst as the results of zero water formation during the methanation reaction. Increasing Ru content to 10% further led to increased WGS reaction and formation of water. Also; the residual chloride ions from the Ru-precursor form a barrier between the support and the metal, and thus both inhibit CO and hydrogen chemisorption on the catalyst surface.

4. Conflicts of interest

The authors declare that they have no competing interests.

5. Acknowledgments

This work was supported by the labs of the Egyptian Petroleum Research Institute (EPRI).

6. Funding

This research did not receive any specific grant from funding agencies in the public, commercial, or not-for-profit sectors.

7. References

[1] Ebiad MA, Abd El-Hafiz DR, Elsalamony RA, Mohamed LS. Ni supported high surface area CeO_2-ZrO_2 catalysts for hydrogen production from ethanol steam reforming. RSC Advances, 2, 8145–56 (2012).

[2] Elsalamony RA, Abd El-Hafiz DR, Ebiad MA, Mansour AM, Mohamed LS. Enhancement of hydrogen production via hydrogen peroxide as an oxidant. RSC Advances, 3, (2013).

[3] Abd El-Hafiz DR, Ebiad MA, Elsalamony RA, Mohamed LS. Highly stable nano Ce-La catalyst for hydrogen production from bio-ethanol. RSC Advances, 5, 4292–303 (2015).

[4] Abd El-Hafiz DR, Ebiad MA, El-Salamony RA. Hydrogen selectivity and carbon behavior during gasoline steam reforming over nano-Al_2O_3 catalysts. Materials for Renewable and Sustainable Energy, 3, 34 (2014).

[5] Bard AJ, Fox MA, Izumi Y. Recent advances in the photocatalytic conversion of carbon dioxide to fuels with water and/or hydrogen using solar energy and beyond. Coordination Chemistry Reviews, 257, 171–86 (2013).

[6] Bard AJ, Fox MA. Artificial Photosynthesis: Solar Splitting of Water to Hydrogen and Oxygen. Accounts of Chemical Research, 28, 141–5 (1995).

[7] Tada S, Ikeda S, Shimoda N, Honma T, Takahashi M, Nariyuki A, Satokawa S. Sponge Ni catalyst with high activity in CO_2 methanation. International Journal of Hydrogen Energy, 42, 30126–34 (2017).

[8] Miao B, Ma SSK, Wang X, Su H, Chan SH. Catalysis mechanisms of CO_2 and CO

methanation. Catalysis Science and Technology, 6, 4048–58 (2016).

[9] El-Salamony RA, El-Temtamy SA, El Naggar AMA, Ghoneim SA, Abd El-Hafiz DR, Ebiad MA, Gendy T, Al-Sabagh AM. Valuation of catalytic activity of nickel–zirconia-based catalysts using lanthanum co-support for dry reforming of methane. International Journal of Energy Research, 45(3), 3899–3912 (2021).

[10] Abd El-Hafiz DR, El-Temtamy SA, Ebiad MA, El-Salamony RA, Ghoniem SA, El Naggar AMA, Gendy TS. Novel LaNi intercalated Egyptian bentonite clay for direct conversion of methane using CO2 as soft oxidant. International Journal of Hydrogen Energy, 45, 9783–94 (2020).

[11] Gendy, T.S., El-Temtamy, S.A., El-Salamony, R.A., Ghoneim SA. Comparative assessment of response surface methodology quadratic models and artificial neural network method for dry reforming of natural gas. Energy Sources, Part A: Recovery, Utilization and Environmental Effects, 40, 1573–82 (2018).

[12] Vance CK, Bartholomew CH. Hydrogenation of carbon dioxide on group viii metals. III, Effects of support on activity/selectivity and adsorption properties of nickel. Applied Catalysis, 7, 169–77 (1983).

[13] Jiménez V, Sánchez P, Panagiotopoulou P, Valverde JL, Romero A. Methanation of CO, CO_2 and selective methanation of CO, in mixtures of CO and CO_2, over ruthenium carbon nanofibers catalysts. Applied Catalysis A: General, 390, 35–44 (2010).

[14] El-Salamony RA, El-Sharaky SA, Al-Temtamy SA, Ahmed M. Al-Sabagh AM, Killa HM. CO_2 valorization into synthetic natural gas (SNG) using a Co–Ni bimetallic Y_2O_3 based catalysts. International Journal of Chemical Reactor Engineering, (2021) https://doi.org/10.1515/ijcre-2020-0163

[15] Kim HY, Lee HM, Park JN. Bifunctional mechanism of CO_2 methanation on Pd-MgO/SiO_2 catalyst: Independent roles of MgO and Pd on CO_2 methanation. Journal of Physical Chemistry C, 114, 7128–31 (2010).

[16] Wang W, Wang S, Ma X, Gong J. Recent advances in catalytic hydrogenation of carbon dioxide. Chemical Society Reviews, 40, 3703–27 (2011).

[17] Wambach J, Baiker A, Wokaun A. CO_2 hydrogenation over metal/zirconia catalysts. Physical Chemistry Chemical Physics, 1, 5071–80 (1999).

[18] Inui T, Kitagawa K, Takeguchi T, Hagiwara T, Makino Y. Hydrogenation of carbon dioxide to C1-C7 hydrocarbons via methanol on composite catalysts. Applied Catalysis A, General, 94, 31–44 (1993).

[19] Saeidi S, Amin NAS, Rahimpour MR. Hydrogenation of CO_2 to value-added products - A review and potential future developments. Journal of CO2 Utilization, 5, 66–81 (2014).

[20] Ganesh I. Conversion of carbon dioxide into methanol - A potential liquid fuel: Fundamental challenges and opportunities (a review). Renewable and Sustainable Energy Reviews, 31, 221–57 (2014).

[21] Liu P, Zhao B, Li S, Shi H, Ma M, Lu J, Yang F, Deng X, Jia X, Ma X, Yan X. Influence of the Microstructure of Ni-Co Bimetallic Catalyst on CO Methanation. Industrial and Engineering Chemistry Research, 59, 1845–54 (2020).

[22] Sabatier P. & SJB. New synthesis of methane. CR Acad. Sci. Paris, 134, 514–6 (1902).

[23] Baraj E, Vagaský S, Hlinčík T, Ciahotný K, Tekáč V. Reaction mechanisms of carbon dioxide methanation. Chemical Papers, 70, 395–403 (2016).

[24] Kang SH, Ryu JH, Kim JH, Seo SJ, Yoo YD, Sai Prasad PS, Lim HJ, Byun CD. Co-methanation of CO and CO_2 on the NiX-Fe1-X/Al_2O_3 catalysts; effect of Fe contents. Korean Journal of Chemical Engineering, 28, 2282–6 (2011).

[25] Graf F, Götz M, Koch AM. State of the Art and Perspectives of CO_2 Methanation Process Concepts for Power-to-Gas Applications State of the Art and Perspectives of CO_2 Methanation Process Concepts for Power-to-Gas Applications, 2014.

[26] Jürgensen L, Ehimen EA, Born J, Holm-Nielsen JB. Dynamic biogas upgrading based on the Sabatier process: Thermodynamic and dynamic process simulation. Bioresource Technology, 178, 323–9 (2015).

[27] Belov I, Vermeiren V, Paulussen S, Bogaerts A. Carbon dioxide dissociation in a microwave plasma reactor operating in a wide pressure range and different gas inlet configurations. Journal of CO_2 Utilization, 24, 386–97 (2018).

[28] Pandey D, Ray K, Bhardwaj R, Bojja S, Chary KVR, Deo G. Promotion of unsupported nickel catalyst using iron for CO2 methanation. International Journal of Hydrogen Energy, 43, 4987–5000 (2018).

[29] Xu S, Chansai S, Shao Y, Xu S, Wang Y chi, Haigh S, Mu Y, Jiao Y, Stere CE, Chen H, Fan X, Hardacre C. Mechanistic study of non-thermal plasma assisted CO_2 hydrogenation over Ru supported on MgAl layered double hydroxide. Applied Catalysis B: Environmental, 268, 118752 (2020).

[30] Baddour FG, Roberts EJ, To AT, Wang L, Habas SE, Ruddy DA, Bedford NM, Wright J, Nash CP, Schaidle JA, Brutchey RL, Malmstadt N. An Exceptionally Mild and Scalable Solution-Phase Synthesis of Molybdenum Carbide Nanoparticles for Thermocatalytic CO_2 Hydrogenation. Journal of the American Chemical Society, 142, 1010–9 (2020).

[31] Witte J, Kunz A, Biollaz SMA, Schildhauer TJ. Direct catalytic methanation of biogas – Part II: Techno-economic process assessment and feasibility reflections. Energy Conversion and Management, 178, 26–43 (2018).

[32] Gao J, Wang Y, Ping Y, Hu D, Xu G, Gu F, Su F. A thermodynamic analysis of methanation reactions of carbon oxides for the production of synthetic natural gas. RSC Advances, 2, 2358–68 (2012).

[33] Aldana PAU, Ocampo F, Kobl K, Louis B, Thibault-Starzyk F, Daturi M, Bazin P, Thomas S, Roger AC. Catalytic CO_2 valorization into CH_4 on Ni-based ceria-zirconia. Reaction mechanism by operand IR spectroscopy, Catalysis Today, 15 October 2013, Elsevier, pp.201–7.

[34] Chang FW, Kuo MS, Tsay MT, Hsieh MC. Hydrogenation of CO_2 over nickel catalysts on rice husk ash-alumina prepared by incipient wetness impregnation. Applied Catalysis A: General, 247, 309–20 (2003).

[35] Yu Y, Chan YM, Bian Z, Song F, Wang J, Zhong Q, Kawi S. Enhanced performance and selectivity of CO_2 methanation over g-C_3N_4 assisted synthesis of Ni–CeO_2 catalyst: Kinetics and DRIFTS studies. International Journal of Hydrogen Energy, 43, 15191–204 (2018).

[36] Simon Q, Barreca D, Bekermann D, Gasparotto A, MacCato C, Comini E, Gombac V, Fornasiero P, Lebedev OI, Turner S, Devi A, Fischer RA, Van Tendeloo G. plasma-assisted synthesis of Ag/ZnO nanocomposites: First example of photo-induced H_2 production and sensing. International Journal of Hydrogen Energy, 36, 15527–37 (2011).

[37] Ocampo F, Louis B, Roger AC. Methanation of carbon dioxide over nickel-based Ce0.72Zr0.28O2 mixed oxide catalysts prepared by sol-gel method. Applied Catalysis A: General, 369, 90–6 (2009).

[38] Liu H, He D. Properties of Ni/Y_2O_3 and its catalytic performance in methane conversion to syngas. International Journal of Hydrogen Energy, 36, 14447–54 (2011).

[39] Muroyama H, Tsuda Y, Asakoshi T, Masitah H, Okanishi T, Matsui T, Eguchi K. Carbon dioxide methanation over Ni catalysts supported on various metal oxides. Journal of Catalysis, 343, 178–84 (2016).

[40] Zhao K, Wang W, Li Z. Highly efficient Ni/ZrO2 catalysts prepared via combustion method for CO2 methanation. Journal of CO_2 Utilization, 16, 236–44 (2016).

[41] Agnelli M, Kolb M, Mirodatos C. Co Hydrogenation on a Nickel Catalyst: 1. Kinetics and Modeling of a Low-Temperature Sintering Process. Journal of Catalysis, 148, 9–21 (1994).

[42] Tada S, Ochieng OJ, Kikuchi R, Haneda T, Kameyama H. Promotion of CO_2 methanation activity and CH_4 selectivity at low temperatures over Ru/CeO_2/Al_2O_3 catalysts. International Journal of Hydrogen Energy, 39, 10090–100 (2014).

[43] Liu Q, Gao J, Zhang M, Li H, Gu F, Xu G, Zhong Z, Su F. Highly active and stable Ni/γ-Al_2O_3 catalysts selectively deposited with CeO_2 for CO methanation. RSC Advances, 4, 16094–103 (2014).

[44] Zeng Y, Ma H, Zhang H, Ying W, Fang D. Highly efficient $NiAl_2O_4$-free Ni/γ-Al_2O_3 catalysts prepared by solution combustion method for CO methanation. Fuel, 137, 155–63 (2014).

[45] Rotgerink HGJL, Mercera PDL, van Ommen JG, Ross JRH. Studies on the promotion of nickel-alumina coprecipitated catalysts. I. Titanium oxide. Applied Catalysis, 45, 239–56 (1988).

[46] Ahn H, Lee KS, Kim M, Lee J. Control of a reactive batch distillation process using an iterative learning technique. Korean J. Chem. Eng, 31, 6–11 (2014).

[47] Gao J, Liu Q, Gu F, Liu B, Zhong Z, Su F. Recent advances in methanation catalysts for the production of synthetic natural gas. RSC Advances, 5, 22759–76 (2015).

[48] Zhang J, Xin Z, Meng X, Lv Y, Tao M. Effect of MoO3 on the heat resistant performances of nickel-based MCM-41 methanation catalysts. Fuel, 116, 25–33 (2014).

[49] Hu D, Gao J, Ping Y, Jia L, Gunawan P, Zhong Z, Xu G, Gu F, Su F. Enhanced investigation of CO methanation over Ni/Al_2O_3 catalysts for synthetic natural gas production. Industrial and Engineering Chemistry Research, 51, 4875–86 (2012).

[50] Zhi G, Guo X, Guo X, Wang Y, Jin G. Effect of La2O3 modification on the catalytic performance of Ni/SiC for methanation of carbon dioxide. Catalysis Communications, 16, 56–9 (2011).

[51] Finch JN, Ripley DL. United States Patent 3988334, 1976.

[52] Kustov AL, Frey AM, Larsen KE, Johannessen T, Nørskov JK, Christensen CH. CO methanation over supported bimetallic Ni-Fe catalysts: From computational studies towards catalyst optimization. Applied Catalysis A: General, 320, 98–104 (2007).

[53] Kuśmierz M. Kinetic study on carbon dioxide hydrogenation over Ru/γ-Al_2O_3 catalysts. Catalysis Today, 137, 429–32 (2008).

[54] Kwak JH, Kovarik L, Szanyi J. CO_2 reduction on supported Ru/Al2O3 catalysts: Cluster size dependence of product selectivity. ACS Catalysis, 3, 2449–55 (2013).

[55] Takeishi K, Aika K ich. Comparison of carbon dioxide and carbon monoxide with respect to hydrogenation on Raney ruthenium catalysts. Applied Catalysis A, General, 133, 31–45 (1995).

[56] Hasan M, Muroyama H, Tsuda Y, Asakoshi T, Masitah H, Okanishi T, Matsui T, Eguchi K. Carbon dioxide methanation over Ni catalysts supported on various metal oxides. Article in Journal of Catalysis, (2016).

[57] Guilera J, Del Valle J, Alarcón A, Díaz JA, Andreu T. Metal-oxide promoted Ni/Al_2O_3 as CO_2 methanation micro-size catalysts. Journal of CO_2 Utilization, 30, 11–7 (2019).

[58] Abu Bakar WAW, Ali R, Toemen S. Catalytic methanation reaction over supported nickel-ruthenium oxide base for purification of simulated natural gas. Scientia Iranica, 19, 525–34 (2012).

[59] Kowalczyk Z, Stołecki K, Raróg-Pilecka W, Miśkiewicz E, Wilczkowska E, Karpiński Z. Supported ruthenium catalysts for selective methanation of carbon oxides at very low CO_x/H_2 ratios. Applied Catalysis A: General, 342, 35–9 (2008).

[60] Luo L, Li S, Zhu YU. The effects of yttrium on the hydrogenation performance and surface properties of a ruthenium-supported catalyst. J. Serb. Chem. Soc, 70, 1419–25 (2005).

[61] Yuan C, Yao N, Wang X, Wang J, Lv D, Li X. The SiO2 supported bimetallic Ni-Ru particles: A good sulfur-tolerant catalyst for methanation reaction. Chemical Engineering Journal, 260, 1–10 (2015).

[62] Zhen W, Li B, Lu G, Ma J. Enhancing catalytic activity and stability for CO_2 methanation on Ni-Ru/γ-Al_2O_3via modulating impregnation sequence and controlling surface-active species Enhancing catalytic activity and stability for CO_2 methanation on Ni-Ru/g-Al_2O_3 via modulating i. (2014).

[63] König CFJ, Schildhauer TJ, Nachtegaal M. Methane synthesis and sulfur removal over a Ru catalyst probed in situ with high sensitivity X-ray absorption spectroscopy. Journal of Catalysis, 305, 92–100 (2013).

[64] Lin C, Zhang C, Lin J. Sol-gel derived Y_2O_3 as an efficient bluish-white phosphor without metal activator ions. Journal of Luminescence, 129, 1469–74 (2009).

[65] Wang Z, Xu H, Zhang Z, Wang S, Ding L, Zeng Q, Yang L, Pei T, Liang X, Gao M, Peng L-M. Growth and Performance of Yttrium Oxide as an Ideal High-κ Gate Dielectric for Carbon-Based Electronics. ACS Publications, 10, 2024–30 (2010).

[66] Kodo M, Soga K, Yoshida H, Yamamoto T. Doping effect of divalent cations on sintering of polycrystalline yttria. Journal of the European Ceramic Society, 30, 2741–7 (2010).

[67] Wu X, Kawi S. Steam reforming of ethanol to H_2 over Rh/Y_2O_3: Crucial roles of Y_2O_3 oxidizing ability, space velocity, and H2/C, Energy and Environmental Science, 2010, pp.334–42.

[68] Wang Y, Wang W, Hong X, Li Y, Zhang Z. Yttrium-stabilized zirconia-promoted metallic nickel catalysts for the partial oxidation of methane to hydrogen. International Journal of Hydrogen Energy, 34, 2252–9 (2009).

[69] Bukhari SN, Chong CC, Teh LP, Vo DVN, Ainirazali N, Triwahyono S, Jalil AA, Setiabudi HD. Promising hydrothermal technique for efficient CO2 methanation over Ni/SBA-15. International Journal of Hydrogen Energy, 44, 20792–804 (2019).

[70] Morsi RE, El-salamony RA. Effect of cationic, anionic and non-ionic polymeric surfactants on the stability, photo-catalytic and antimicrobial activities of yttrium oxide nano fluids. Journal of Molecular Liquids, 297, 111848 (2020).

[71] Liu A, Praserthdam S, Phatanasri S. Investigation on the increased stability of the Ni–Co bi-metallic catalysts for the carbon

dioxide reforming of methane. Catalysis Today, (2019).

[72] Chen X, Zou H, Chen S, Dong X, Lin W. Selective Oxidation of CO in Excess H_2 over Ru/Al2O3 Catalysts Modified with Metal Oxide. Journal of Natural Gas Chemistry, 16, 409–14 (2007).

[73] Sun GB, Hidajat K, Wu XS, Kawi S. A crucial role of surface oxygen mobility on nanocrystalline Y_2O_3 support for oxidative steam reforming of ethanol to hydrogen over Ni/Y_2O_3 catalysts. Applied Catalysis B: Environmental, 81, 303–12 (2008).

[74] Basahel SN, Mokhtar M, Alsharaeh EH, Ali TT, Mahmoud HA, Narasimharao K. Physico-Chemical and Catalytic Properties of Mesoporous CuO-ZrO_2 Catalysts. mdpi.com, 6, (2016).

[75] El Naggar AMA, Gobara HM, Sayed HA El, Soliman FS. New advances in hydrogen production via the catalytic decomposition of wax by-products using nanoparticles of SBA frame-worked MoO_3. Elsevier, 106, 615–24 (2015).

[76] El-Salamony RA, Gobara HM, Younis SA. Potential application of MoO_3 loaded SBA-15 photo-catalyst for removal of multiple organic pollutants from water environment. Journal of Water Process Engineering, 18, 102–12 (2017).

[77] Chen X hu, Zhang P ze, Wei D bo, Huang X, Ding F, Li F kun, Dai X jun, Wang Z zhong. Correlation between crystal structure and mechanical performance of Cr-implanted 300M high-strength steel using X-ray diffraction method. Journal of Iron and Steel Research International, 26, 1106–16 (2019).

[78] Liu H, Wu H, He D. Methane conversion to syngas over Ni/Y_2O_3 catalysts - Effects of calcination temperatures of Y_2O_3 on physicochemical properties and catalytic performance. Fuel Processing Technology, 119, 81–6 (2014).

[79] Ssing K, Everett D, Haul R, Moscou L, Pierotti R, Rouquerol J, Siemieniewsks T. Reporting physisorption data for gas/solid system. Pure and Applied Chemistry, 57, 603–19 (1985).

[80] Shalaby NH, Elsalamony RA, El Naggar AMA. Mesoporous waste-extracted SiO2-Al2O3-supported Ni and Ni-H3PW12O40 nano-catalysts for photo-degradation of methyl orange dye under UV irradiation. New Journal of Chemistry, 42, 9177–86 (2018).

[81] Shan W, Luo M, Ying P, Shen W, Li C. Reduction property and catalytic activity of Ce1-XNiXO2 mixed oxide catalysts for CH4 oxidation. Applied Catalysis A: General, 246, 1–9 (2003).

[82] Li G, Hu L, Hill JM. Comparison of reducibility and stability of alumina-supported Ni catalysts prepared by impregnation and co-precipitation. Applied Catalysis A: General, 301, 16–24 (2006).

[83] Liu H, He D. Properties of Ni/Y2O3 and its catalytic performance in methane conversion to syngas. International Journal of Hydrogen Energy, 36, 14447–54 (2011).

[84] Passos FB, Oliveira ER, Mattos L V, Noronha FB. Effect of the support on the mechanism of partial oxidation of methane on platinum catalysts. Springer, 110, 161–7 (2006).

[85] Sun GB, Hidajat K, Wu XS, Kawi S. A crucial role of surface oxygen mobility on nanocrystalline Y_2O_3 support for oxidative steam reforming of ethanol to hydrogen over Ni/Y_2O_3 catalysts. Applied Catalysis B: Environmental, 81, 303–12 (2008).

[86] Granger P, Delannoy L, Leclercq L, Leclercq G. On the effect of deactivation on the kinetics of CO oxidation by NO over Pt-Rh catalysts. Journal of Catalysis, 177, 147–51 (1998).

[87] Zafeiropoulos G, Nikolopoulos N, Kordouli E, Sygellou L, Bourikas K, Kordulis C, Lycourghiotis A. Developing Nickel-Zirconia Co-Precipitated Catalysts for Production of Green Diesel. mdpi.com, 9, (2019).

[88] Ji L, Lin J, Zeng HC. Thermal processes of volatile RuO_2 in nanocrystalline Al_2O_3 matrixes involving $\gamma \rightarrow \alpha$ phase transformation. Chemistry of Materials, 13, 2403–12 (2001).

[89] Williams CT, Takoudis CG, Weaver MJ. Methanol oxidation on rhodium as probed by surface-enhanced Raman and mass spectroscopies: Adsorbate stability, reactivity, and catalytic relevance. Journal of Physical Chemistry B, 102, 406–16 (1998).

[90] Xirong Chen, Hanbo Zou, Shengzhou Chen XDWL. Selective Oxidation of CO in Excess H2over Ru/Al_2O_3CatalystsModified with Metal Oxide. Journal of Natural Gas Chemistry, 16, 409–414 (2007).

[91] Stuchinskaya TL, Musawir M, Kozhevnikova EF, Kozhevnikov I V. Liquid-phase oxidation of alcohols by oxygen and nitrous oxide catalysed by Ru-Co oxide. Journal of Catalysis, 231, 41–7 (2005).

[92] Li F, Chen J, Zhang Q, Wang Y. Hydrous ruthenium oxide supported on CO_3O_4 as

efficient catalyst for aerobic oxidation of amines. Green Chemistry, 10, 553–6 (2008).

[93] Zhang N, Du Y, Yin M, Guan C, Feng J, Li D. Facile synthesis of supported RuO_2·: X H2O nanoparticles on Co-Al hydrotalcite for the catalytic oxidation of alcohol: Effect of temperature pretreatment. RSC Advances, 6, 49588–96 (2016).

[94] Mazzieri VA, Coloma-Pascual F, Mazzieri V, Coloma-Pascual F, Arcoya A, L'argentière A PC, Fígoli NS. Alkyne selective hydrogenation View project Composite materials for selective hydrogenation View project XPS, FTIR, and TPR characterization of Ru/Al 2 O 3 catalysts. Elsevier, (2003).

[95] Bossi A, Garbassi F, Orlandi A, Petrini G, Zanderighi L. Preparation aspects of Ru-supported catalysts and their influence on the final products. Studies in Surface Science and Catalysis, 3, 405–16 (1979).

[96] He Z, Wang X, Liu R, Gao S, Xiao T. Performances of different additives on NiO/γ-Al_2O_3 catalyst in CO methanation. Applied Petrochemical Research, 6, 235–41 (2016).

[97] Bartholomew CH, Farrauto RJ. Chemistry of nickel-alumina catalysts. Journal of Catalysis, 45, 41–53 (1976).

[98] Diskin A, Cunningham R, Today RO-C, 1998 U. The oxidative chemistry of methane over supported nickel catalysts. Catalysis Today, 46, 147–54 (1998).

[99] Mazzieri VA, Coloma-Pascual F, Mazzieri V, Coloma-Pascual F, Arcoya A, L'argentière A PC, Fígoli NS. Alkyne selective hydrogenation View project Composite materials for selective hydrogenation View project XPS, FTIR and TPR characterization of Ru/Al_2O_3 catalysts. (2003).

[100] Moulder JF, Stickle WF, Sobol PE, Bomben KD. Handbook of X-ray photoelectron spectroscopy; Chastain, J. Perkin-Elmer Corp., Eden Prairie, MN, (1992).

[101] Morgan DJ. Resolving ruthenium: XPS studies of common ruthenium materials. Surface and Interface Analysis, 47, 1072–9 (2015).

[102] Froment P, Genet MJ, Devillers M. Surface reduction of ruthenium compounds with long exposure to an X-ray beam in photoelectron spectroscopy. Journal of Electron Spectroscopy and Related Phenomena, 104, 119–26 (1999).

[103] Kim YI, Hatfield WE. Electrical, magnetic, and spectroscopic properties of tetrathiafulvalene charge transfer compounds with iron, ruthenium, rhodium and iridium halides. Inorganica Chimica Acta, 188, 15–24 (1991).

[104] Moulder JF. Handbook of X-ray photoelectron spectroscopy. Physical electronics, 230–2 (1995).

[105] Uwamino Y, Ishizuka T, Yamatera H. X-ray photoelectron spectroscopy of rare-earth compounds. Journal of Electron Spectroscopy and Related Phenomena, 34, 67–78 (1984).

[106] Basińska A, Stoch J, Domka F. XPS study of Ru/Fe2O3 catalysts for the water-gas shift reaction. Polish Journal of Environmental Studies, 12, 395–400 (2003).

[107] Kim KS, Gossmann AF, Winograd N. X-ray photoelectron spectroscopic studies of palladium oxides and the palladium-oxygen electrode. Analytical Chemistry, 46, 197–200 (1974).

[108] Nesbitt HW, Legrand D, Bancroft GM. Interpretation of Ni2p XPS spectra of Ni conductors and Ni insulators. Physics and Chemistry of Minerals, 27, 357–66 (2000).

[109] Jiang D, Yang Y, Huang C, Huang M, Chen J, Rao T, Ran X. Removal of the heavy metal ion nickel (II) via an adsorption method using flower globular magnesium hydroxide. Journal of Hazardous Materials, 373, 131–40 (2019).

[110] Huang H, Sun X, Wang S, Liu Y, Li X, Liu J, Kang Z, Lee S-T. Cite this: Dalton Trans. 40, 11362 (2011).

[111] Huang H, Sun X, Wang S, Liu Y, Li X, Liu J, Kang Z, Lee ST. Strong red emission of pure Y2O3 nanoparticles from oxygen-related defects. Dalton Transactions, 40, 11362–6 (2011).

[112] Van TT, Chang JP. Radical-enhanced atomic layer deposition of Y_2O_3 via a β-diketonate precursor and O radicals. Surface Science, 596, 1–11 (2005).

[113] Garbarino G, Riani P, Magistri L, Busca G. A study of the methanation of carbon dioxide on Ni/Al2O 3 catalysts at atmospheric pressure. International Journal of Hydrogen Energy, 39, 11557–65 (2014).

[114] Aziz MAA, Jalil AA, Triwahyono S, Saad MWA. CO_2 methanation over Ni-promoted mesostructured silica nanoparticles: Influence of Ni loading and water vapor on activity and response surface methodology studies. Chemical Engineering Journal, 260, 757–64 (2015).

[115] Borgschulte A, Gallandat N, Probst B, Suter R, Callini E, Ferri D, Arroyo Y, Erni R, Geerlings H, Züttel A. Sorption enhanced CO_2 methanation. Physical Chemistry Chemical Physics, 15, 9620 (2013).

[116] Mills GA, Steffgen FW. Catalytic methanation. Catalysis Reviews, 8, 159–210 (1974).
[117] Peebles DE, Goodman DW, White JM. Methanation of carbon dioxide on Ni(100) and the effects of surface modifiers. Journal of Physical Chemistry, 87, 4378–87 (1983).
[118] Eckle S, Anfang H-G, Behm RJ. Reaction Intermediates and Side Products in the Methanation of CO and CO_2 over Supported Ru Catalysts in H_2 -Rich Reformate Gases. The Journal of Physical Chemistry C, 115, 1361–7 (2011).
[119] Borgschulte A, Gallandat N, Probst B, Suter R, Callini E, Ferri D, Arroyo Y, Erni R, Geerlings H, Züttel A. Sorption enhanced CO_2 methanation. Physical Chemistry Chemical Physics, 15, 9620–5 (2013).
[120] Akamaru S, Shimazaki T, Kubo M, Abe T. Density functional theory analysis of methanation reaction of CO_2 on Ru nanoparticle supported on TiO_2 (101). Applied Catalysis A: General, 470, 405–11 (2014).
[121] Batista MS, Santiago EI, Assaf EM, Ticianelli EA. Evaluation of the water-gas shift and CO methanation processes for purification of reformate gases and the coupling to a PEM fuel cell system. Journal of Power Sources, 145, 50–4 (2005).
[122] Tian D, Liu Z, Li D, Shi H, Pan W, Cheng Y. Bimetallic Ni-Fe total-methanation catalyst for the production of substitute natural gas under high pressure. Fuel, 104, 224–9 (2013).
[123] Tandon PK, Bahadur Singh S, Kumar Tandon P. Catalysis: A brief review on Nano-Catalyst. Journal of Energy and Chemical, 2, 106–15 (2014).
[124] Yu Y, Jin G, Wang Y, Guo X. Synthesis of natural gas from CO methanation over SiC supported Ni-Co bimetallic catalysts. Catalysis Communications, 31, 5–10 (2013).
[125] Wang S, Lu GQ. Role of CeO_2 in Ni/CeO_2-Al_2O_3 catalysts for carbon dioxide reforming of methane. Applied Catalysis B: Environmental, 19, 267–77 (1998).
[126] Liu H, Zou X, Wang X, Lu X, Ding W. Effect of CeO_2 addition on Ni/Al_2O_3 catalysts for methanation of carbon dioxide with hydrogen. Journal of Natural Gas Chemistry, 21, 703–7 (2012).
[127] Nurunnabi M, Murata K, Okabe K, Inaba M, Takahara I. Performance and characterization of Ru/Al_2O_3 and Ru/SiO_2 catalysts modified with Mn for Fischer-Tropsch synthesis. Applied Catalysis A: General, 340, 203–11 (2008).